

Denoising and Interpolation of Noisy Bayer Data with Adaptive Cross-Color Filters

Dmitriy Paliy^a, Alessandro Foi^a, Radu Bilcu^b, and Vladimir Katkovnik^a

^aInstitute of Signal Processing, Tampere University of Technology, P.O. Box 553, FIN-33101 Tampere, Finland. e-mail: firstname.lastname@tut.fi

^bNokia Research Center, Tampere, Finland. e-mail: firstname.lastname@nokia.com

ABSTRACT

We propose a novel approach for joint denoising and interpolation of noisy Bayer-patterned data acquired from a digital imaging sensor (e.g., CMOS, CCD). The aim is to obtain a full-resolution RGB noiseless image. The proposed technique is specifically targeted to filter signal-dependant, e.g. Poissonian, or heteroscedastic noise, and effectively exploits the correlation between the different color channels. The joint technique for denoising and interpolation is based on the concept of local polynomial approximation (LPA) and intersection of confidence intervals (ICI). These directional filters utilize simultaneously the green, red, and blue color channels. This is achieved by a linear combination of complementary-supported smoothing and derivative kernels designed for the Bayer data grid. With these filters, the denoised and the interpolated estimates are obtained by convolutions over the Bayer data. The ICI rule is used for data-adaptive selection of the length of the designed cross-color directional filter. Fusing estimates from multiple directions provides the final anisotropic denoised and interpolated values. The full-size RGB image is obtained by placing these values into the corresponding positions in the image grid. The efficiency of the proposed approach is demonstrated by experimental results with simulated and real camera data.

Keywords: Bayer pattern, color filter array interpolation, spatially adaptive denoising, sensor noise

1. INTRODUCTION

In digital imaging systems, the image formation is a complex process. The light passes through the optical system of the camera and is focused on the digital sensor (e.g., a CCD or CMOS sensor). The sensor is composed of photon-collection pixels covered with a color filter array (CFA). Each pixel works as a photon-counter to measure the amount of light coming to it. The color filter array is used to sample different spectral components, thus each pixel measures the amount of light at a particular spectral range. For example, the Bayer CFA samples the coming light into red, green, and blue components¹ according to a checkerboard rectangular sampling grid. It is the most widespread CFA nowadays and therefore in this paper we focus mainly on it. The sensor produces a digital value for each pixel which corresponds to the intensity of the light at that position. This digital output of the sensor is called “raw data”. The raw data from the sensor is always corrupted by random noise, which is predominantly signal-dependent, following the Poissonian distribution^{2,3,4,5}.

The problem is to restore the true full-color and full-resolution image from the noisy subsampled data. The conventional approach used in image reconstruction chains for raw sensor data applies successively denoising and demosaicing steps. Usually, the denoising step comes first. This choice was supported by experimental analysis⁶ and motivated by the fact that knowledge about the noise model is of great importance in denoising and this knowledge is more accurate and precise at the raw-data level. Demosaicing algorithms are then used to reconstruct missing red, green, and blue values to produce an RGB image. It is essentially an interpolation problem, thus demosaicing is also known as color filter array interpolation (CFAI). Most CFAI techniques are designed for noiseless data^{7,8,9}.

The latest works^{10,11,12,13}, have shown that performing the demosaicing and interpolation jointly is more efficient than treating them as independent procedures.

In particular, noting that image interpolation and image denoising are both estimation problems, the papers^{10,11} propose a unified approach to perform demosaicing and denoising simultaneously. The multi-color

demosaicing/denoising problem is simplified as a single-color denoising problem and a total least-squares algorithm is designed to solve this problem.

In^{12,13}, we proposed to perform denoising and demosaicing jointly by filtering the initial directional interpolated estimates of noisy color intensities. These estimates are first decorrelated by a color transformation operator and then denoised by directional anisotropic adaptive filters. This approach is found to be efficient in attenuating both noise and interpolation errors. The exploited denoising technique is based on the local polynomial approximation (LPA) where the adaptivity to data is provided by multiple hypothesis-testing exploiting the intersection of confidence intervals (ICI) rule, which is applied for the adaptive selection of varying scales (window sizes) of the LPA¹⁴.

The technique proposed in the present paper is essentially different from our previous contributions^{12,13}, as here we do not require some initial directional estimates of the decorrelated color channels. Instead, we design directional varying-scale joint denoising/interpolation filtering kernels, which are applied directly on the Bayer data. These kernels work simultaneously on the different color channels, thus they automatically and effectively exploit the high correlation between the channels. We call these kernels *LPA cross-color filters*. Specifically, the LPA cross-color filters are a linear combination of LPA smoothing kernels and LPA derivative kernels with complementary supports. For example, noise-free (denoised) estimates of the green at green positions (i.e., on the green subdomain of the pattern) are obtained with cross-color kernels which combine a smoothing kernel for the green, supported on the green subdomain, and a derivative estimation kernel for the red/blue, supported on the red/blue subdomain. Analogously, noise-free (interpolated) estimates of the green at red/blue positions (i.e., where the green is missing) are also obtained with cross-color kernels which combine a smoothing kernel for the green, supported on the green subdomain, and a derivative estimation kernel for the red/blue, supported on the red/blue subdomain. However, the resulting cross-color kernels for these two cases are different, because the subdomains are displaced with respect to the estimation point. The estimates are obtained by convolutions of the cross-color kernels over the Bayer data. The ICI rule is used for data-adaptive selection of the length of the designed cross-color directional kernel. Fusing estimates obtained from multiple directions provides us with higher-quality estimates that correspond to denoised and interpolated values. Finally, the full-size RGB image is obtained by placing the estimated values into the corresponding positions in the image grid.

We remark that contrary to conventional filtering techniques, which are designed for stationary Gaussian noise, our technique is specifically designed for treating signal-dependent noise such as the Poissonian one, characteristic of the raw data from CCD and CMOS digital image sensors.

This new approach based on cross-color filters leads to reduced computational complexity and memory load. We show by experiments that the proposed joint denoising and demosaicing technique performs, at a lower computational cost, better or comparable than combination of successive state-of-the-art techniques targeted denoising and demosaicing, and achieves comparable performance to the best joint denoising and demosaicing techniques known to the authors. We support the experiments with real data simulations taken from a camera phone equipped with CMOS sensor, showing the feasibility of the proposed technique for commercial applications.

2. IMAGE FORMATION MODEL

2.1. Bayer Mask Sampling

The CFA is a crucial element in design of single-sensor digital cameras. Different characteristics in design of CFA affect both performance and computational efficiency of the demosaicing solution^{15,16}. The Bayer CFA¹ (Fig.1a) samples red (R), green (G), and blue (B) colors arranged in a checkerboard pattern. Study on a variety of R, G, and B sampling patterns may be found in¹⁵. Alternative approaches include the complementary mosaic pattern, which contains cyan, yellow, magenta, and green photosites¹⁷, and the recently proposed CFA with transparent elements¹⁸, which is supposed to improve the signal-to-noise ratio (SNR) of the acquired data.

However, the Bayer CFA is still the most widely used and therefore our technique is developed for this

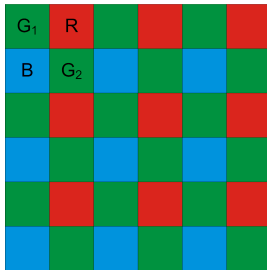


Figure 1. Bayer color filter array.

particular CFA. The general Bayer sampling operator \mathcal{B} is defined as

$$\mathcal{B}\{y_{RGB}\}(x) = \begin{cases} G(x), & \text{if } x \in X_{G_1} \\ G(x), & \text{if } x \in X_{G_2} \\ R(x), & \text{if } x \in X_R \\ B(x), & \text{if } x \in X_B \end{cases}, \quad x \in X, \quad (1)$$

where $y_{RGB} = (R, G, B)$ is a full-color RGB image, R (red), G (green), and B (blue) are the color channels,

$$\begin{aligned} X_{G_1} &= \{(x_1, x_2) : x_1 = 1, 3, \dots, 2N - 1, x_2 = 1, 3, \dots, 2M - 1\} \\ X_{G_2} &= \{(x_1, x_2) : x_1 = 2, 4, \dots, 2N, x_2 = 2, 4, \dots, 2M\} \\ X_R &= \{(x_1, x_2) : x_1 = 1, 3, \dots, 2N - 1, x_2 = 2, 4, \dots, 2M\} \\ X_B &= \{(x_1, x_2) : x_1 = 2, 4, \dots, 2N, x_2 = 1, 3, \dots, 2M - 1\} \end{aligned}$$

are the spatial subdomains of the available R , G , and B samples, and

$$X = X_{G_1} \cup X_{G_2} \cup X_R \cup X_B = \{x = (x_1, x_2) : x_1 = 1, \dots, 2N, x_2 = 1, \dots, 2M\} \subset \mathbb{N}^2$$

is the $2N \times 2M$ domain of the image. Note that the green channel is sampled on two subdomains G_1 and G_2 .

Demosaicing aims at inverting \mathcal{B} , in order to reconstruct $R(x)$, $G(x)$, and $B(x)$ intensities at every $x \in X$ from the mosaic $\mathcal{B}\{y_{RGB}\}$.

2.2. Additive Noise Models

Any image recorded by a digital camera sensor is noisy. We consider the generic heteroscedastic additive noise model

$$z(x) = \mathcal{B}\{y_{RGB}\}(x) + \sigma(x)\eta(x), \quad x \in X, \quad (2)$$

where z is the recorded noisy signal, $\mathcal{B}\{y_{RGB}\}$ is the noise-free Bayer data, $\sigma : X \rightarrow \mathbb{R}^+$ is a deterministic function, η is an independent zero-mean random noise with variance equal to one at every point $x \in X$. Thus, $\sigma(x)$ is the standard deviation of $z(x)$ at x . Our problem is to reconstruct the full-resolution RGB image y_{RGB} from the noisy subsampled data z .

For instance, as a trivial example, if $\sigma(x) = \text{const}$ and $\eta(x) \sim \mathcal{N}(0, 1)$, $\forall x \in X$, then (2) is the conventional additive white Gaussian noise model.

However, in practice, $\sigma(x)$ is not necessarily constant with respect to the spatial variable x . The following noise models are particular instances of (2), which are more relevant to the CFAI problem:

a) The signal-dependent Poissonian model of the form $\chi z(x) \sim \mathcal{P}(\chi \mathcal{B}\{y_{RGB}\}(x))$, $\chi > 0$, is considered in this work. This noise can be written explicitly in the additive form (2) where the standard deviation depends on the image intensity as

$$\sigma(x) = \text{std}\{z(x)\} = \sqrt{(\mathcal{B}\{y_{RGB}\}(x)) / \chi}. \quad (3)$$

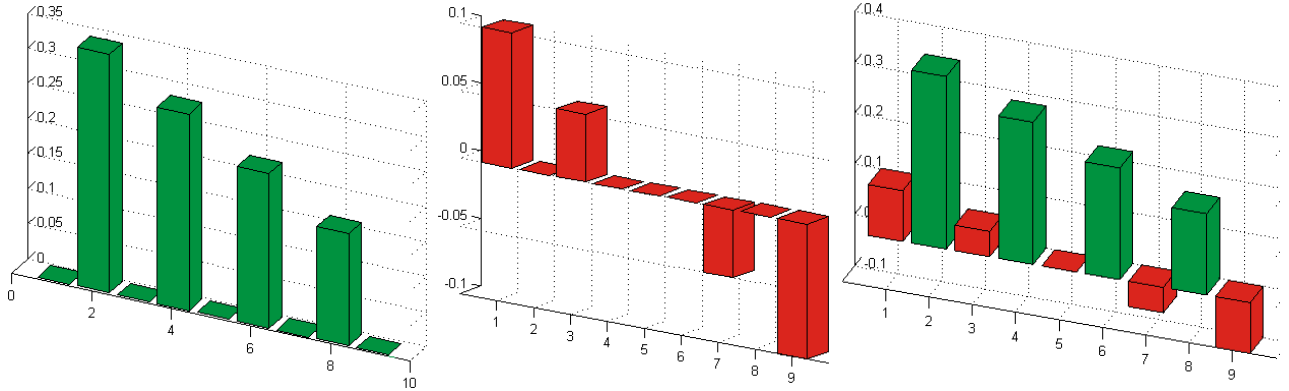


Figure 2. Directional linear filter designed for Bayer pattern: a) Linear combination of zero and first orders subsampled LPA filters $(1 - \alpha)g_{0,s,\theta}^{(0)} + \alpha g_{1,s,\theta}^{(0)}$; b) Differentiation LPA filter $g_{1,s,\theta}^{(1)}$; c) Linear filter as a combination of smoothing (a) and differentiation (b) designed for Bayer pattern.

Here χ is a parameter that controls the noisiness of the observed data z . It is shown in^{2,3} that such a model can be used for generic CCD/CMOS digital imaging sensors.

b) The nonstationary Gaussian noise with the signal-dependant standard deviation^{10,11}

$$\sigma(x) = k_0 + k_1 y(x), \quad \eta(x) \sim \mathcal{N}(0, 1), \quad (4)$$

where, k_0 and k_1 are the parameters that control the noisiness of the observed data $z(x)$.

A more sophisticated model for CCD/CMOS sensor noise as a combination of Poissonian and Gaussian noises, where effects of under- and over-exposure (e.g., saturation or clipping) are taken into account, is proposed in⁴. The authors also propose a technique to determine the noise model parameters from any single observation.

3. DESIGN OF DIRECTIONAL LINEAR FILTERS AND INTERPOLATORS IN POLYNOMIAL BASIS

For the filtering, a bank of linear filters with directional non-symmetrical kernels $g_{s,\theta}$ is obtained by LPA.

A rotated directional non-symmetric kernel $g_{s,\theta}$ is used with the angle θ which defines the directionality of the filter, and s is a length of the kernel support (or a scale parameter of the kernel) in this direction. The directionality of the kernel is defined by the non-symmetric window-function used in the LPA. The technical details about generating the LPA kernels on the subsampled grid can be found in¹³, where notations are the same as in this paper.

Different kernels $g_{s,\theta}$ should be used for denoising of given subsampled data and for interpolation of missing data. In practice, we use rotated line-wise non-symmetrical 1D kernels $g_{s,\theta}(x)$ of width equal to one.

Further, for denoising we use eight directional estimates for $\theta \in \tilde{\Theta} = \{k\pi/4 : k = 0, \dots, 7\}$, while for interpolation we use only four directions $\theta \in \Theta = \{k\pi/2 : k = 0, \dots, 3\}$.

3.1. Design of Interpolation Kernels

Let us denote the convolutional 1D kernel as $g_{m,s,\theta}^{(k)}$, where we use m to indicate the LPA polynomial order, k as an index of the estimated derivative, and $\theta \in \tilde{\Theta}$. Then, the designed kernel is given as a linear combination

$$\bar{g}_{s,\theta} = (1 - \alpha)g_{0,s,\theta}^{(0)} + \alpha g_{1,s,\theta}^{(0)} + \beta g_{1,s,\theta}^{(1)}, \quad (5)$$

where $g_{0,s,\theta}^{(0)}$ and $g_{1,s,\theta}^{(0)}$ are smoothing kernels of zero and first order defined on \mathbb{Z}^2 , respectively, and $g_{1,s,\theta}^{(1)}$ is a differentiating kernel of first order. The parameter $\alpha \in [0, 1]$ defines proportions of the zero and first order

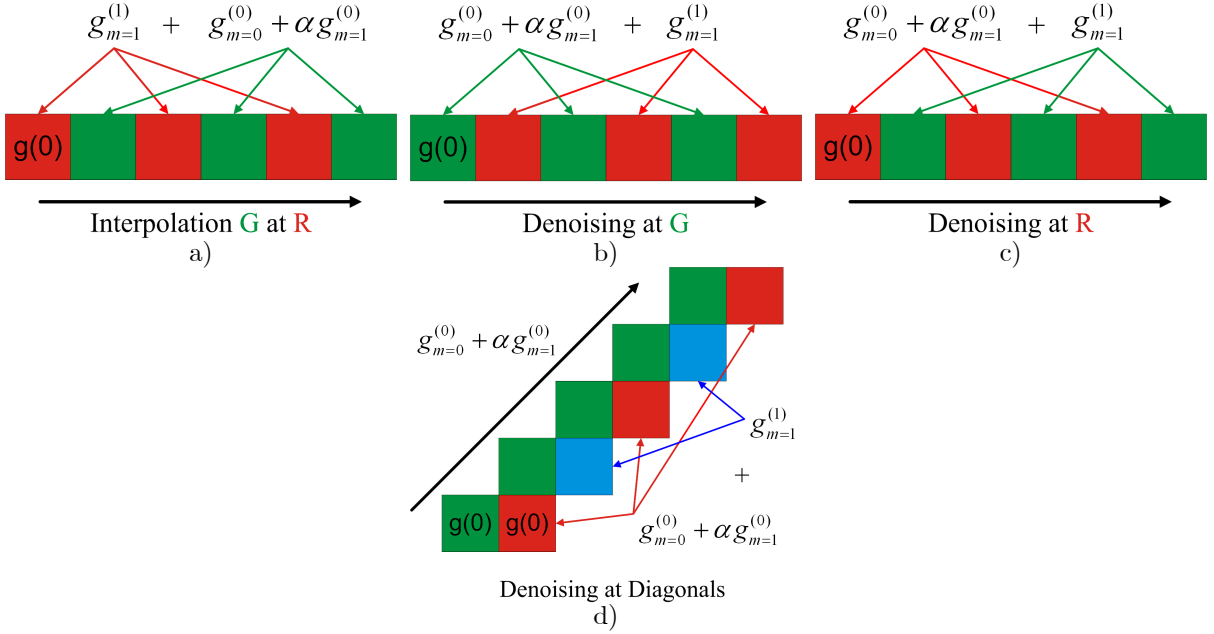


Figure 3. Directional LPA kernels designed for Bayer pattern. Horizontal and vertical directions: a) Interpolation of Green color at Red position; b) Denoising kernel for Green; c) Denoising kernel for Red; d) Denoising at diagonals is performed differently for Green and Red/Blue.

smoothing estimates. The parameter β is a weight of the derivative estimates. The kernels $g_{0,s,\theta}^{(0)}$, $g_{1,s,\theta}^{(0)}$ and $g_{1,s,\theta}^{(1)}$ have different supports (non-zero elements) and work with different color components.

The LPA filter is realized by the convolution of z against the kernel:

$$(\bar{g}_{s,\theta} \otimes z)(x) = \sum_v z(x) \bar{g}_{s,\theta}(x-v). \quad (6)$$

In Fig.2, we illustrate an interpolation kernel of green G at a position $x \in X_R$. The kernels are colored to the respective colors. The smoothing kernels $g_{0,s,\theta}^{(0)}(x-\cdot)$ and $g_{1,s,\theta}^{(0)}(x-\cdot)$ are supported on the grid of green X_G while the differentiating kernel $g_{1,s,\theta}^{(1)}(x-\cdot)$ is supported on the grid of red X_R . Fig.2a shows a smoothing kernel $(1-\alpha)g_{0,s,\theta}^{(0)} + \alpha g_{1,s,\theta}^{(0)}$ for G at R positions, while Fig.2b shows a scaled differentiation kernel $\beta g_{1,s,\theta}^{(1)}$ at R (at R positions). Their combination $\bar{g}_{s,\theta}$ as in (5) is shown in (Fig.2c). After the translation*, all these kernels have their origin at $x \in X_R$.

Fig.3 provides further illustration of these kernels (particularly Fig.3a), where the origin is marked by " $g(0)$ ".

3.2. Design of Denoising Kernels

In order to perform the denoising of the Bayer pattern data, we design the kernel as a linear combination of smoothing and differentiating kernels, similarly to (5),

$$\tilde{g}_{s,\theta} = (1-\alpha)g_{0,s,\theta}^{(0)} + \alpha g_{1,s,\theta}^{(0)} + \beta g_{1,s,\theta}^{(1)}, \quad (7)$$

where $\theta \in \tilde{\Theta}$. However, here the supports are different from those used for interpolation. For instance (see Fig.3b), for denoising of green the smoothing kernels $g_{0,s,\theta}^{(0)}(x-\cdot)$ and $g_{1,s,\theta}^{(0)}(x-\cdot)$ are supported at X_G and equal to zero for the complementary grid $X \setminus X_G$. At the same time the differentiating kernel $g_{1,s,\theta}^{(1)}(x-\cdot)$ is supported

*Translation is embedded in the convolution (6).

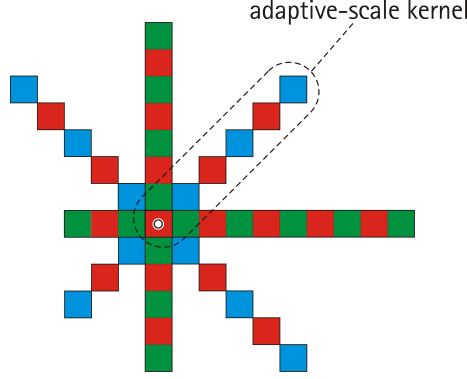


Figure 4. Denoising at R position with directional filtering.

on X_R for using the red channel for green data filtering and equal to zero for the complementary grid $X \setminus X_R$. After the translation, all these kernels have their origin at $x \in X_G$.

Similarly, we consider denoising of red in Fig.3c. The smoothing kernels $g_{0,s,\theta}^{(0)}(x-\cdot)$, $g_{1,s,\theta}^{(0)}(x-\cdot)$ are supported on X_R while the differentiating kernel $g_{1,s,\theta}^{(1)}(x-\cdot)$ is supported on X_G . After the translation, all these kernels have their origin at $x \in X_R$. Other color combinations can be illustrated in a similar way.

Diagonal directions require different consideration. In Fig.3d the denoising for the diagonal is illustrated for green and red channels. There is no downsampling for the green G color channel at diagonal directions. As a result we use only smoothing kernels

$$\tilde{g}_{s,\theta} = (1 - \alpha)g_{0,s,\theta}^{(0)} + \alpha g_{1,s,\theta}^{(0)}. \quad (8)$$

For denoising the red R and blue B channels (Fig.3d), we use full combined kernels using the smoothing and differentiating kernels (7).

4. DIRECTIONAL DENOISING AND INTERPOLATION WITH ADAPTIVE WINDOW-SIZE

We exploit the ICI criterion¹⁴ in order to adaptively select the length of the cross-color kernels for both denoising and interpolation. For a fixed direction θ and at a fixed pixel position x , the procedure is implemented as follows. The denoising and interpolation estimates $\tilde{y}_{s,\theta}(x)$, $\bar{y}_{s,\theta}(x)$ are calculated for an ordered set $S = \{s_1, s_2, \dots, s_J\}$ of window sizes, $s_1 < s_2 < \dots < s_J$, as the convolution of the corresponding cross-color kernels against the noisy Bayer data:

$$\tilde{y}_{h,\theta}(x) = (\tilde{g}_{s,\theta} \otimes z)(x), \quad \bar{y}_{s,\theta}(x) = (\bar{g}_{s,\theta} \otimes z)(x).$$

The standard-deviations $\sigma_{\tilde{y}_{s,\theta}}(x)$ and $\sigma_{\bar{y}_{s,\theta}}(x)$ of the above estimates are computed, respectively, as

$$\sigma_{\tilde{y}_{s,\theta}}(x) = \sqrt{(\tilde{g}_{s,\theta}^2 \otimes \sigma^2)(x)}, \quad \sigma_{\bar{y}_{s,\theta}}(x) = \sqrt{(\bar{g}_{s,\theta}^2 \otimes \sigma^2)(x)}, \quad (9)$$

where σ is the standard deviation of the noise in (2).

For the set of denoising estimates $\{\tilde{y}_{s,\theta}(x)\}_{s \in S}$, let us consider the sequence of confidence intervals

$$\tilde{D}_i = [\tilde{y}_{s,\theta}(x) - \Gamma \sigma_{\tilde{y}_{s,\theta}}(x), \tilde{y}_{s,\theta}(x) + \Gamma \sigma_{\tilde{y}_{s,\theta}}(x)], \quad (10)$$

where i is the index of the scale s , $i = 1, \dots, J$, and $\Gamma > 0$ is a threshold parameter. The ICI rule is stated as follows: consider the intersection of the confidence intervals $I_i = \bigcap_{j=1}^i \tilde{D}_j$, and let i^+ be the largest of the indices i for which I_i is non-empty. Then, the adaptive scale s_θ^+ is defined as $s_\theta^+ = s_{i^+}$ and, as result, the adaptive-scale

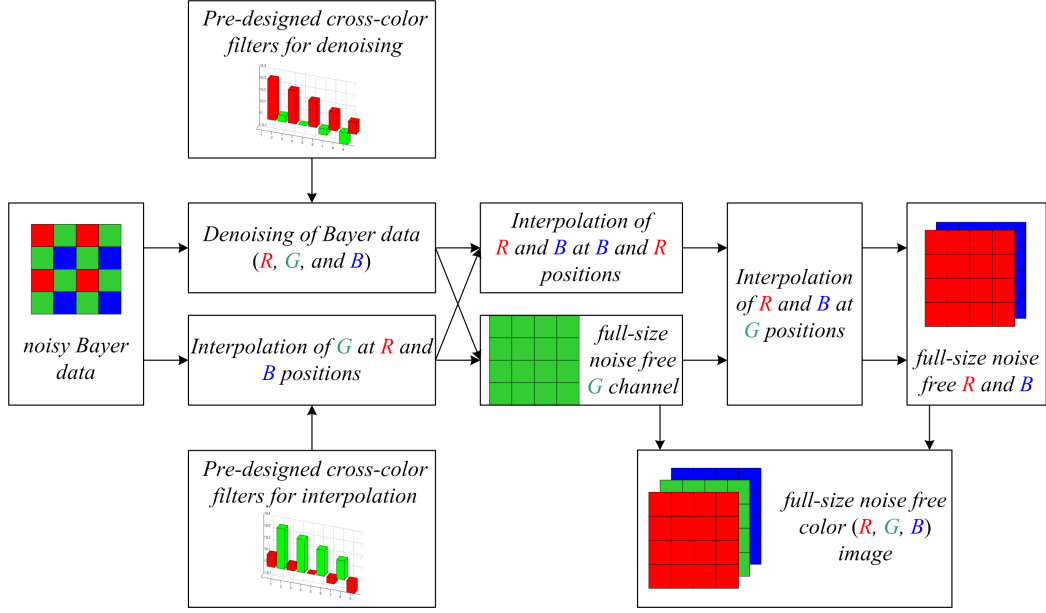


Figure 5. Block diagram of the proposed restoration technique.

denoising estimate is $\tilde{y}_{s_\theta^+, \theta}(x)$. The parameter Γ is a key element of the algorithm as it controls the balance between bias and variance in the adaptive estimates¹⁴. Too large value of this parameter leads to oversmoothing, whereas too small value leaves the noise unfiltered. We treat Γ as a fixed design parameter of the algorithm.

Analogously, for the interpolation estimates $\bar{y}_{s_\theta^+, \theta}(x)$ we can define the confidence intervals

$$\bar{D}_i = [\bar{y}_{s_\theta^+, \theta}(x) - \Gamma \sigma_{\bar{y}_{s_\theta^+, \theta}}(x), \bar{y}_{s_\theta^+, \theta}(x) + \Gamma \sigma_{\bar{y}_{s_\theta^+, \theta}}(x)] \quad (11)$$

and the same criterion as above selects an adaptive-scale interpolation estimate $\bar{y}_{s_\theta^+, \theta}(x)$.

The standard deviations of these adaptive estimates are denoted as $\tilde{\sigma}_{s_\theta^+, \theta}(x)$ and $\bar{\sigma}_{s_\theta^+, \theta}(x)$.

5. ANISOTROPIC DENOISING AND INTERPOLATION

For each point $x \in X$, the ICI rule yields the adaptive-scale estimates for each direction θ . The final anisotropic denoised and interpolated estimates are defined as a combination (aggregation) of the adaptive-scale estimates obtained for the different directions. The union of the supports of $\tilde{g}_{s_\theta^+, \theta}$ can be treated as an approximation of the best local vicinity of x in which the estimation model fits the data (see Fig.4).

To simplify notation, in what follows we drop the subscript s_θ^+ and denote the adaptive scale estimates and their standard-deviations as $\tilde{y}_\theta(x)$, $\tilde{\sigma}_\theta(x)$ (instead of $\tilde{y}_{s_\theta^+, \theta}(x)$, $\tilde{\sigma}_{s_\theta^+, \theta}(x)$) and $\bar{y}_\theta(x)$, $\bar{\sigma}_\theta(x)$ (instead of $\bar{y}_{s_\theta^+, \theta}(x)$, $\bar{\sigma}_{s_\theta^+, \theta}(x)$).

5.1. Anisotropic Denoising of R , G , and B

The anisotropic denoised estimate $\tilde{y}(x)$ at the point $x \in X$ is combined (aggregated) from the directional estimates $\tilde{y}_\theta(x)$ obtained by ICI for $\theta \in \Theta$. Specifically, we use the convex combination

$$\tilde{y}(x) = \sum_{\theta \in \Theta} \frac{\tilde{\sigma}_\theta^{-2}(x) \tilde{y}_\theta(x)}{\sum_{\theta \in \Theta} \tilde{\sigma}_\theta^{-2}(x)}, \quad (12)$$

where $\tilde{y}(x)$ is an estimate $\hat{R}(x)$ of red $R(x)$ for $x \in X_R$ (see example in Fig.4), an estimate $\hat{B}(x)$ of blue $B(x)$ for $x \in X_B$, and estimate $\hat{G}(x)$ of green $G(x)$ for $x \in X_{G_1} \cup X_{G_2}$.

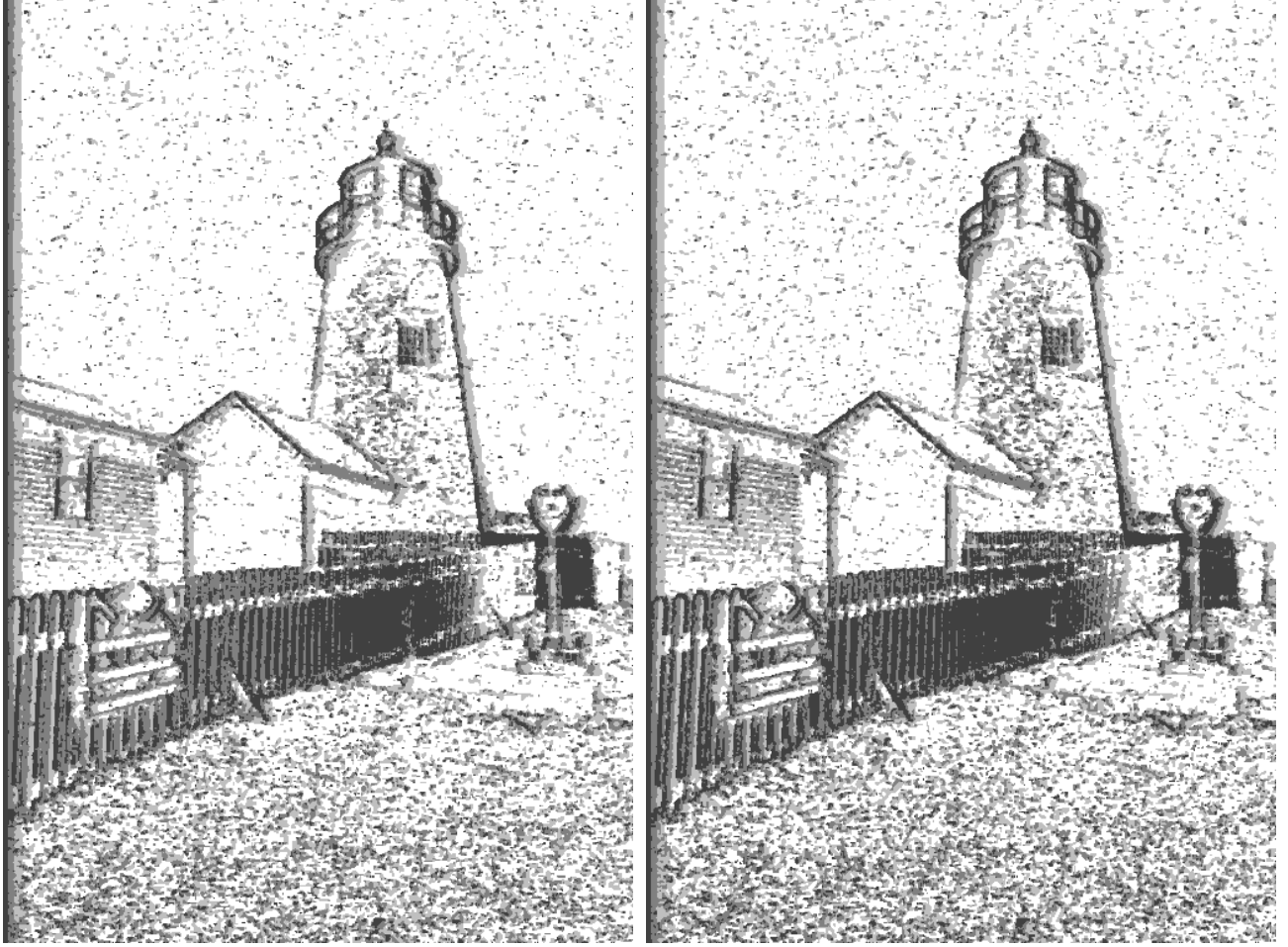


Figure 6. Scales selected by ICI in the horizontal direction ($\theta=0$) for: denoising of Bayer pattern (left); interpolation of Bayer pattern (right).

5.2. Anisotropic Interpolation of G at R and B positions

By aggregating four adaptive directional interpolation estimates we obtain

$$\bar{y}(x) = \sum_{\theta \in \bar{\Theta}} \frac{\bar{\sigma}_{\theta}^{-2}(x) \bar{y}_{\theta}(x)}{\sum_{\theta \in \bar{\Theta}} \bar{\sigma}_{\theta}^{-2}(x)}, \quad (13)$$

where $\bar{y}(x)$ is an estimate $\hat{G}(x)$ of $G(x)$ at $x \in X_R$, and is an estimate $\hat{G}(x)$ of $G(x)$ at $x \in X_B$.

Finally, (12) and (13) yield the fully reconstructed green color channel $\hat{G}(x)$, $\forall x \in X$.

5.3. Interpolation of R and B at B and R positions

It is clear that $\bar{y}(x)$ for $x \in X_{G_1}$ is an estimate $\hat{R}(x)$ of red color, and for $x \in X_{G_2}$ is an estimate $\hat{B}(x)$ of blue color. However, in practice, we found that using the green color estimate $\hat{G}(x)$ for interpolation of R and B at B and R positions, respectively, provides better results than using the red and blue estimates. As a result, interpolation at the mentioned positions is done as follows:

$$\bar{y}_{RB}(x) = (\tilde{y} \otimes g_{RB})(x) + (\hat{G} \otimes g'_G)(x), \quad (14)$$

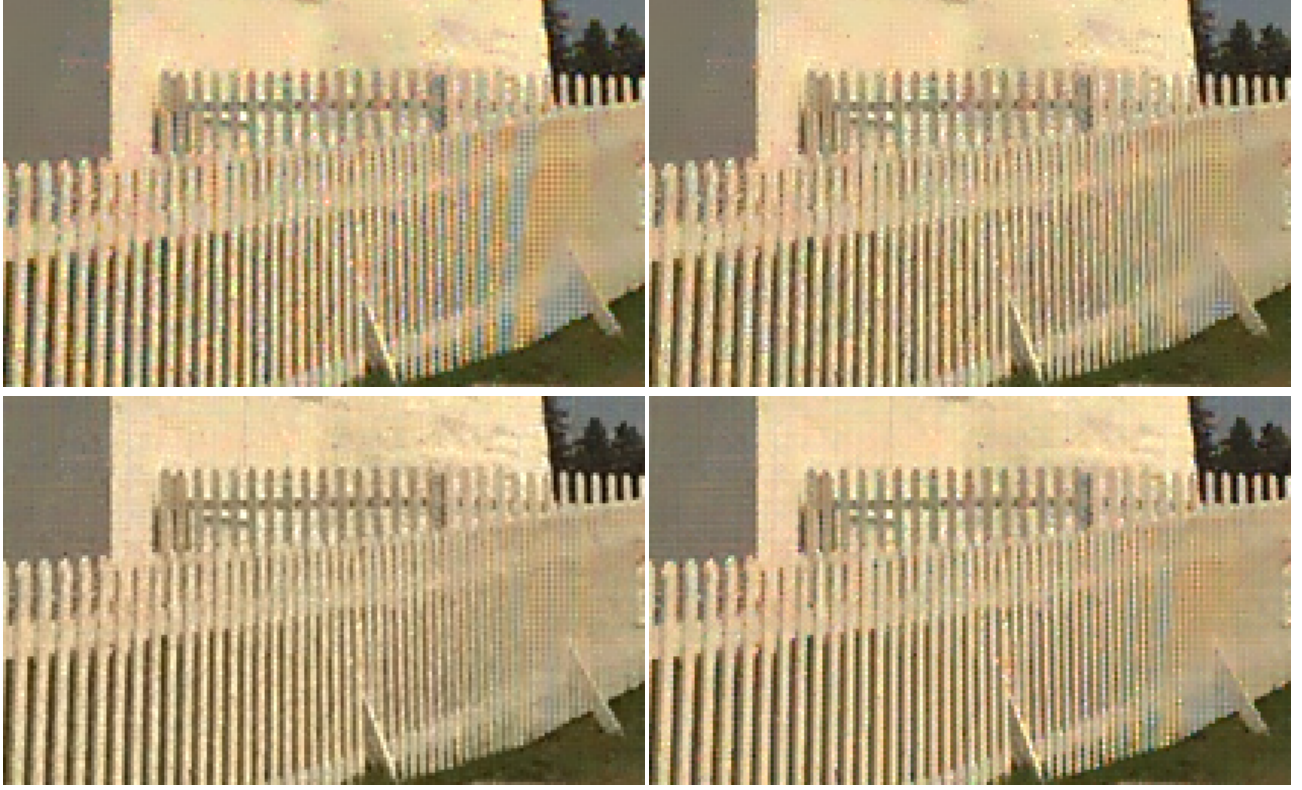


Figure 7. A part of the restored noisy Lighthouse image from the observation subsampled according to the Bayer CFA corrupted by the Poissonian noise. The order is from left to right and from top to bottom: LPA-ICI prefiltering¹⁹ and "Linear interpolation"⁸ CFAI performed as two successive steps, PSNR = (27.88, 29.36, 28.39); LPA-ICI prefiltering¹⁹ and DLMMSE⁹ CFAI performed as two successive steps, PSNR = (28.68, 29.52, 29.59); Integrated Denoising and CFAI based on LPA-ICI¹³, PSNR = (29.39, 30.14, 30.15); Proposed denoising/interpolation, PSNR = (28.70, 29.90, 29.35).

where $x \in X$ and the fixed-size kernels g_{RB} and g'_G are

$$g_{RB} = \begin{bmatrix} 1/4 & 0 & 1/4 \\ 0 & 0 & 0 \\ 1/4 & 0 & 1/4 \end{bmatrix},$$

and

$$g'_G = \frac{1}{4 + 4/\sqrt{2}} \begin{bmatrix} -1/\sqrt{2} & -1 & -1/\sqrt{2} \\ -1 & 4 + 4/\sqrt{2} & -1 \\ -1/\sqrt{2} & -1 & -1/\sqrt{2} \end{bmatrix}.$$

The red color estimate is $\hat{R}(x) = \bar{y}_{RB}(x)$ for $x \in X_B$, and the estimate of blue color $\hat{B}(x)$ at red positions $x \in X_R$ is $\hat{B}(x) = \bar{y}_{RB}(x)$.

5.4. Interpolation of R and B at G positions

Let us define \bar{y}_R as $\bar{y}_R(x) = \hat{R}(x)$ for $x \in X_R \cup X_B$ and $\bar{y}_R(x) = 0$ for $x \in X_{G_1} \cup X_{G_2}$. Similarly, for the blue channel $\bar{y}_B(x) = \hat{B}(x)$ for $x \in X_R \cup X_B$ and $\bar{y}_B(x) = 0$ for $x \in X_{G_1} \cup X_{G_2}$. The interpolation of R/B colors at G positions is performed in a way similar to (14):

$$\begin{aligned} \hat{R}(x) &= (\bar{y}_R \otimes g_G)(x) + (\hat{G} \otimes g'_G)(x), & x \in X_{G_1} \cup X_{G_2}, \\ \hat{B}(x) &= (\bar{y}_B \otimes g_G)(x) + (\hat{G} \otimes g'_G)(x), & x \in X_{G_1} \cup X_{G_2}, \end{aligned}$$






			HA	SA	AP	Linear	CCA+PP	Cross-Color	HD	CCA	DLMMSE	Sp. Adapt.
07		Red	30.07	30.44	30.42	30.51	30.62	<i>30.75</i>	30.76	30.79	30.75	32.04
		Green	31.01	30.87	31.13	31.61	31.30	<i>31.63</i>	31.43	31.51	31.53	31.75
		Blue	29.87	30.68	30.77	31.08	31.15	<i>31.15</i>	31.07	31.39	31.29	32.36
08		Red	25.72	26.63	26.49	24.98	26.60	<i>25.91</i>	26.18	26.42	26.67	27.17
		Green	26.61	27.14	27.16	26.99	27.29	<i>27.32</i>	27.24	27.27	27.45	27.94
		Blue	25.42	26.85	26.56	24.88	26.82	<i>26.00</i>	26.21	26.57	26.81	27.28
13		Red	25.00	26.45	26.07	25.05	26.43	<i>25.64</i>	26.33	26.25	26.34	27.20
		Green	25.60	26.59	26.55	26.38	26.69	<i>26.06</i>	26.81	26.62	26.66	27.30
		Blue	24.93	26.53	26.26	25.12	26.61	<i>25.83</i>	26.47	26.45	26.52	27.11
19		Red	28.17	28.57	28.53	27.88	28.58	<i>28.70</i>	28.48	28.55	28.68	29.39
		Green	29.07	29.26	29.33	29.36	29.38	<i>29.90</i>	29.45	29.38	29.52	30.14
		Blue	28.61	29.50	29.30	28.39	29.46	<i>29.35</i>	29.23	29.35	29.59	30.15
23		Red	31.59	31.68	31.85	31.87	31.81	<i>31.65</i>	32.15	32.13	32.11	32.59
		Green	32.57	32.40	32.56	33.10	32.80	<i>32.71</i>	32.87	33.01	33.02	33.43
		Blue	30.79	31.96	31.85	32.07	32.32	<i>31.96</i>	32.21	32.50	32.49	32.83
Mean PSNR	Red	28.11	28.75	28.67	28.05	28.80	<i>28.52</i>	28.77	28.82	28.91	29.68	
	Green	28.96	29.25	29.34	29.48	29.49	<i>29.53</i>	29.55	29.55	29.63	30.11	
	Blue	27.92	29.10	28.94	28.30	29.27	<i>28.85</i>	29.03	29.25	29.33	29.95	

Table 1. PSNR comparison of demosaicing methods for noisy images corrupted by Poissonian noise. With a pre-processing noise reduction step¹⁹: HA⁷, SA²⁰, AP²¹, Linear⁸, CCA+PP is a demosaicing approach proposed in²³ with postprocessing²², HD¹⁰, CCA is a demosaicing approach proposed in²³, DLMMSE⁹. No pre-processing: Sp. Adapt.¹³, the Cross-Color is proposed in this paper.

where

$$g_G = \begin{bmatrix} 0 & 1/4 & 0 \\ 1/4 & 0 & 1/4 \\ 0 & 1/4 & 0 \end{bmatrix}.$$

Finally, the all three R , G , and B color channels are reconstructed. The block diagram of the proposed technique is shown in Fig.5.

6. RESULTS

We have used the standard test images from the Kodak database with the intensities in the range $[0,255]$. We performed simulations for the noise models (3) and (4). For the presented experiments, we have used $\chi = 0.5447$ for the Poissonian model (3), and $k_0 = 10$, $k_1 = 0.1$ for the model (4).

The use of ICI requires the knowledge of σ . However, it depends on the unknown signal. Therefore, we used rough estimates of the standard deviation σ for (3) as $\hat{\sigma} = \sqrt{z/\chi}$, and for (4) as $\hat{\sigma} = |k_0 + k_1 z|$.

For the LPA-ICI filtering, the threshold parameter Γ is different for denoising and interpolation: $\Gamma = 1$ in (10) for denoising, and $\Gamma = 0.9$ in (11) for interpolation. The scales used for denoising are $S = \{2, 4, 8, 14\}$ and for interpolation are $S = \{3, 5, 9, 15\}$. The parameter α for LPA kernels is equal to 0.15. The parameter $\beta = 1$, but in (7) $\beta = 0.7$ for diagonal directions.

The result of the ICI rule is illustrated in Fig.6 for the Lighthouse test image corrupted by Poissonian noise as in (3). The two figures show the values of adaptive scales selected by the ICI in the horizontal direction $\theta = 0$. These are two full-size images with dimensions $2N \times 2M$. Fig.6(left) and Fig.6(right) correspond to the adaptive scales selected by the ICI at this direction for the denoising and for the interpolation, respectively. It is clearly visible that structures of details, edges, are accurately delineated. Note also that no influence of the Bayer pattern can be seen in the adaptive scales. This is important because it corresponds to suppression of potential color distortions.






		07	08	13	19	23
						
<i>signal dependant noise</i>		$(k_0, k_1) = (10, 0.1)$				
Joint demosaicing and denoising ^{10,11}	R	28.02	22.68	22.98	25.20	29.82
	G	28.39	23.91	23.31	26.48	31.34
	B	28.08	23.00	23.26	26.53	30.27
proposed	R	28.26	23.91	23.68	26.51	29.14
	G	29.01	24.76	23.79	27.54	30.37
	B	28.69	24.14	23.99	27.40	29.55

Table 2. PSNR values for CFA interpolation of images corrupted by noise with $\sigma = k_0 + k_1 \mathcal{B}\{y_{RGB}\}^{10,11}$.

Fig.7 illustrates a part of the Lighthouse image restored by "Linear interpolation"⁸, DLMMSE⁹, integrated denoising and CFAI based on LPA-ICI¹³, and the technique proposed in this work. The CFAI techniques "Linear interpolation"⁸ and DLMMSE⁹ are designed for noiseless data. Therefore, we used denoising designed particularly for Poissonian data¹⁹ as prefiltering. It is an iterative technique and 4 iterations were performed.

The PSNR values in Fig.7 were calculated for the full-size images after borders of width 15 pixels were eliminated, in order to avoid influence of the boundary effect on the PSNR. Here, the integrated denoising and CFAI based on LPA-ICI¹³ shows the best performance among the reviewed methods. However, the technique proposed in this paper is significantly less computationally demanding than¹³ and shows the second best numerical results.

The PSNR values for different CFAI are summarized in Table 1 in the ascending order of Mean PSNR (for 5 images) values. The results for the technique proposed in this paper are highlighted with the italic type. Denoising for Poissonian data¹⁹ was used as prefiltering for all of them with exception of the LPA-ICI based joint demosaicing and denoising (the proposed "Cross-Color" and "Sp. Adapt." given in¹³). It is seen that the proposed technique shows comparable results to more sophisticated CFAI with prefiltering¹⁹ with significantly lower computational complexity. The technique proposed by us in¹³ performs best, but its computational costs are also higher. Comparison for computational complexity is given later.

The simulations Fig.7(top left) and Fig.7(top right) aim at illustrating the performance of the conventional approach of successive denoising and demosaicing. It is seen that results for combination of two very sophisticated techniques (e.g., as in Fig.7(top right)) can be improved with significantly less computational costs as it is shown for the proposed technique.

The comparison for the nonstationary Gaussian noise (4) is given in Table 2. The numerical results (PSNR) are presented for each color R , G , and B channels for 5 test images from standard image testing set. The best results are highlighted with bold face. The superiority of the proposed technique is seen for the most of images.

The evaluation of the computational complexity in terms of processing time shows the efficiency of the proposed technique. In particular[†], the average time for processing a 512×768 image by HA⁷ CFAI with prefiltering¹⁹ (computationally, prefiltering is the most expensive part here, as HA is one of the least expensive adaptive CFAI algorithms) is 220 sec. approximately, for the proposed technique 70 sec., for¹³ 150 sec., and for the joint demosaicing and denoising^{10,11} 1870 sec. The efficiency of the proposed cross-color filters is demonstrated by these times and from the good results shown in the tables and figures.

The restoration of real noisy Bayer raw data from the sensor of a cameraphone is illustrated in Fig.8. The noise model and its parameters were identified exactly in the same way how it is done in^{2,3}. The images at the first row were interpolated by Hamilton-Adams CFAI⁷ and the second row by the proposed CFAI for noisy data. The Hamilton-Adams CFAI⁷ is used only to illustrate the noisiness of the images. The histograms for all images were equalized in order to improve visual perception in the printout. No other color correction steps, or pre- and post-filtering were applied in these experiments.

[†]The simulations were performed in the MATLAB environment (ver. 7.1 SP3) on a PC equipped with a Pentium 4 HT 3.2GHz CPU and 2GB of RAM, and running the Windows XP SP2 operating system.



Figure 8. Fragments of images that illustrate the restoration of real noisy Bayer data measured directly from the sensor of a camera phone: (first row) Hamilton-Adams CFAI⁷; (second row) proposed technique.

The natural question is how the proposed technique performs if there is no noise, i.e. $\sigma(x) = 0, \forall x \in X$. If $\sigma = 0$ then the ICI selects the smallest scales, which is an isotropic analogue of gradient-based (e.g., as in^{7,8}) CFAI.

7. CONCLUSIONS

In this paper, we developed a novel spatially adaptive interpolation for noisy Bayer-patterned Poissonian data and even more general types of heteroscedastic noises, i.e. noises whose variance is defined as an arbitrary function defined on the image domain (image-dependent as well as image-independent). This technique is based on the novel filtering and interpolating kernels essentially exploiting the color correlation of signals. The ICI algorithm is used for spatially adaptive selection of the window sizes for these kernels. The LPA kernels were designed in such a way, that they simultaneously exploit two color channels for each direction. This approach results in higher efficiency of data utilization and in better suppression of distortions at edges.

8. ACKNOWLEDGMENTS

This work was supported by the Finnish Funding Agency for Technology and Innovation (Tekes), AVIPA2 project, and by the Academy of Finland, project No. 213462 (Finnish Centre of Excellence program 2006-2011).

REFERENCES

1. Bayer, B.E., "Color imaging array," U.S. Patent 3 971 065, July 1976.

2. Foi, A., V. Katkovnik, D. Paliy, K. Egiazarian, M. Trimeche, S. Alenius, R. Bilcu, M. Vehvilainen, "Apparatus, method, mobile station and computer program product for noise estimation, modeling and filtering of a digital image", U.S. Patent (Applications no. 11/426,128, June 2006, and no. 11/519,722, Sep. 2006).
3. Foi, A., S. Alenius, V. Katkovnik, and K. Egiazarian, "Noise measurement for raw-data of digital imaging sensors by automatic segmentation of non-uniform targets", *IEEE Sensors Journal*, vol. 7, no. 10, pp. 1456-1461, October 2007.
4. Foi, A., M. Trimeche, V. Katkovnik, and K. Egiazarian, "Practical Poissonian-Gaussian noise modeling and fitting for single image raw-data", to appear in *IEEE Trans. Image Process.*
5. Bovik, A., *Handbook of Image and Video Processing*, New York: Academic, 2000.
6. Kalevo, O., H. Rantanen, "Noise Reduction Techniques for Bayer-Matrix Images," Sensors and Camera systems for scientific, industrial, and digital photography applications III, Proceedings of SPIE vol. 4669, 2002.
7. Hamilton, J.F., Jr., and J.E. Adams, "Adaptive color plane interpolation in single color electronic camera," U.S. Patent 5 629 734, May 1997.
8. Malvar, H.S., L.-W. He, and R. Cutler, "High-quality linear interpolation for demosaicing of Bayer-patterned color images," IEEE Int Conf (ICASSP '04), Proceedings on Acoustics, Speech, and Signal Processing 3, pp. 485-488, 2004.
9. Zhang, L., X. Wu, "Color demosaicking via directional linear minimum mean square-error estimation," *IEEE Trans. on Image Processing*, vol. 14, no. 12, pp. 2167-2178, 2005.
10. Hirakawa, K., T.W. Parks, "Joint Demosaicing and Denoising," IEEE ICIP 2005, III, pp. 309-312, 2005.
11. Hirakawa, K., T.W. Parks, "Joint Demosaicing and Denoising," *IEEE Trans. Image Processing*, August 2006. (MATLAB files available at <http://www.accidentalmark.com/research/>)
12. Paliy, D., M. Trimeche, V. Katkovnik, S. Alenius, "Demosaicing of Noisy Data: Spatially Adaptive Approach," Proc. SPIE Electronic Imaging 2007, Computational Imaging IV, 6497-20, San Jose, CA, January 2007.
13. Paliy, D., V. Katkovnik, R. Bilcu, S. Alenius, K. Egiazarian, "Spatially Adaptive Color Filter Array Interpolation for Noiseless and Noisy Data," *Int. J. Imaging Syst. Technol., Sp. Iss. on Applied Color Image Processing*, vol. 17, no. 3, pp. 105-122, October 2007.
14. Katkovnik, V., K. Egiazarian, and J. Astola, *Local Approximation Techniques in Signal and Image Processing*, SPIE Press, Monograph Vol. PM157, September 2006.
15. Lukac, R., K.N. Plataniotis, "Color filter arrays: design and performance analysis," *IEEE Trans. on Consumer Electronics*, vol. 51, no. 4, pp. 1260-1267, 2005.
16. Adams, J., K. Parulski, and K. Spaulding, "Color processing in digital cameras," *IEEE Micro*, vol. 18, no. 6, pp. 20-30, 1998.
17. Parulski, K., K.E. Spaulding, *Color image processing for digital cameras*, In 'Digital Color Imaging Handbook', (ed.) G. Sharma, CRC Press, Boca Raton, FL, pp. 728-757, 2002.
18. Luo, G., "A Novel Color Filter Array with 75% Transparent Elements," Digital Photography III, Proc. of SPIE-IS&T Electronic Imaging, vol. 6502, 65020T.
19. Foi, A., R. Bilcu, V. Katkovnik, and K. Egiazarian, "Anisotropic local approximations for pointwise adaptive signal-dependent noise removal," Proc XIII European Signal Process Conf, EUSIPCO 2005.
20. Xin Li, "Demosaicing by successive approximation," *IEEE Tran. on Image Processing*, vol. 14, no. 3, pp. 370-379, March 2005.
21. Gunturk, B.K., Y. Altunbasak, R.M. Mersereau, "Color plane interpolation using alternating projections," *IEEE Trans. on Image Processing*, vol. 11, no. 9, pp. 997-1013, September 2002.
22. Lukac, R., Martin K., Plataniotis K.N., "Demosaicked Image Postprocessing Using Local Color Ratios," *IEEE Trans. on Circuits and Systems for Video Technology*, vol. 14, no. 6, pp. 914-920, June 2004.
23. Lukac, R., Plataniotis K.N., Hatzinakos D., Aleksic M., "A Novel Cost Effective Demosaicing Approach," *IEEE Trans. on Consumer Electronics*, vol. 50, no. 1, pp. 256-261, February 2004.